Robotics and Autonomous Systems 62 (2014) 1597–1609

Contents lists available at ScienceDirect

Robotics and Autonomous Systems

journal homepage: www.elsevier.com/locate/robot

A leader-following trajectory generator with application to quadrotor formation flight

V. Roldão [a], R. Cunha [a,*], D. Cabecinhas [a,b], C. Silvestre [a,b], P. Oliveira [a]

[a] Department of Electrical Engineering and Computer Science, and Institute for Systems and Robotics, Instituto Superior Técnico, Universidade de Lisboa, 1046-001 Lisbon, Portugal

[b] Department of Electrical and Computer Engineering, Faculty of Science and Technology, University of Macau, Av. Padre Tomás Pereira, Taipa, Macau, China

HIGHLIGHTS

- We present a strategy for real-time generation of multi-vehicle formation trajectories.
- Rich leader–follower formation trajectories with varying curvatures between vehicles are obtained.
- The trajectory generator in conjunction with a trajectory tracking controller is applied to formation flight of quadrotors.
- Simulation and experimental results are presented to illustrate the effectiveness of the proposed solution.

ARTICLE INFO

Article history:
Received 2 October 2013
Received in revised form
9 April 2014
Accepted 5 May 2014
Available online 14 May 2014

Keywords:
Trajectory generation
Leader–follower
Formation flight
Nonlinear control
Lyapunov methods
Autonomous vehicles
Quadrotors

ABSTRACT

This paper presents a strategy for real-time generation of formation trajectories using a leader–follower approach. A trajectory generator prescribes the motion of a group of virtual vehicles, using a Lyapunov-based nonlinear controller that stabilizes the position of the leader in the reference frame of the virtual vehicles at a predefined distance vector. This strategy differs from the standard approach of defining the desired distance vector in an inertial frame and can be used to obtain rich formation trajectories with varying curvatures between vehicles. By imposing adequate constraints on the motion of the virtual vehicles, the generation of valid formation trajectories is naturally guaranteed, bypassing the demanding task of obtaining complete path descriptions. The trajectories are generated online and provided to a trajectory tracking controller specifically designed for quadrotor vehicles. Simulation and experimental flight tests are presented to evaluate the performance of the solution proposed, applied to formation control of quadrotors.

1. Introduction

The problem of controlling multiple vehicles to perform cooperative tasks poses important challenges to automatic control. It has been the scope of a number of publications and experimental results are beginning to appear (see [1] for a survey on the topic and [2–7] for more specific examples). Cooperative control of multi-vehicle systems has proven to be advantageous in carrying out a variety of tasks such as surveillance and area exploration [3], where it results in a faster and more efficient process, or load transportations [4], where the use of multiple vehicles allows for a reduction in the size of the platforms. Within the field of cooperative control, the problem of maintaining a multi-vehicle formation while moving in space, known as formation control, has received considerable attention, with several methodologies proposed over the past 15 years, including the behavioral approach [8], potential-field and graph theory methods [9–11], and leader–follower strategies [12–16].

The leader–follower approach is particularly attractive due to its simplicity and scalability. It has been applied to different vehicles, including mobile robots [12–14], AUVs [15], and UAVs [16]. It consists in ensuring that one or more follower vehicles converge to and maintain a desired distance and orientation relative to a leader vehicle, whose trajectory may not be known a priori. Its scalability derives from the fact that each follower can become the leader for additional vehicles and the process can be repeated. A characterization of the error amplification with respect to leader inputs and

* Corresponding author. Fax: +351 218418291.
E-mail address: rita@isr.ist.utl.pt (R. Cunha).

http://dx.doi.org/10.1016/j.robot.2014.05.002
0921-8890/

disturbances, and stability analysis of leader–follower formations in cascaded form can be found in [12].

In this paper, we adopt a leader–follower approach and focus on generating rich formation trajectories, in the sense that the followers can describe trajectories that differ considerably from that of the leader, namely in terms of curvature. The proposed trajectory generator is vehicle independent and takes the form of a nonlinear control law, which stabilizes, at a predefined distance vector, the position of the leader in the body frame of a virtual follower. Then, a trajectory tracking controller uses the generated trajectories as references for real vehicles. This strategy differs from the majority of approaches found in the literature, which define the desired distance vector in either the body frame of the leader (see [12–14], for examples applied to unicycles) or the inertial frame (see [17], for an example applied to quadrotors). Notice that the latter can only be used to define formations where the followers describe an offset version of the leader's trajectory. In contrast, by imposing adequate kinematic constraints on the motion of the virtual vehicles, the current approach gives rise to curvature-rich formation trajectories that are naturally acquired without the need to explicitly compute the path parameters of the leader.

The solution proposed exhibits some additional properties of interest. Given that the leader–follower distance is expressed in the body frame of the follower, relative position measurements can be directly acquired by sensors installed onboard the follower vehicles. Also, the trajectories are generated at runtime, based solely on the motion of the leader, which is tracking a pre-assigned trajectory unknown to the followers. As such, deviations in the leader's motion are captured by the trajectory generator and the trajectories to be tracked are changed accordingly.

The adopted approach of defining the position error in the body frame of the follower dictates the existence of an inner dynamics given by the angular distance between vehicles, whose boundedness must be guaranteed in order to generate valid formation trajectories. Such a result is ensured by imposing adequate constraints on the motion of the virtual vehicles and guaranteeing that well-defined conditions relating the curvature of the leader's trajectory and the desired distance between vehicles are satisfied, so that stabilizing the position of the leader in the body frame of the virtual follower naturally entails an attitude stabilization.

To derive the control law for both trajectory generation and trajectory tracking, we resort to the Lyapunov-based backstepping technique. Backstepping is a well known technique extensively used for control of nonlinear systems [18]. The backstepping procedure can be complemented by other methodologies to obtain additional characteristics for the control law. In the proposed trajectory generation controller, we combine backstepping with the use of integral control to achieve rejection of constant disturbances, as discussed in [19]. The trajectory tracking controller presented builds on the solution proposed in [20] for quadrotor vehicles and adopts the principle of assigning an appropriate thrust and using the torque actuation to ensure convergence to an appropriate thrust direction. Using an alternative and simpler saturated control law, global trajectory tracking is guaranteed together with boundedness of the thrust actuation.

The resulting methodology is experimentally validated in a rapid prototyping and testing architecture based on the Matlab/Simulink environment, which integrates navigation data from a VICON motion capture system [21], the control algorithms, and the communications with three radio controlled Blade mQX quadrotors [22]. In the experiment presented, the leader vehicle tracks a figure eight trajectory and is followed by the other two vehicles in a tight triangle formation that imposes significant curvature variations on the described trajectories.

This paper is structured as follows. Section 2 contains a description of the strategy adopted for leader-following trajectory generation. Section 3 presents the solution proposed for flight formation applied to quadrotors. The quadrotor dynamic model is described and a control law for trajectory tracking is derived and tested in simulation. Section 4 contains the experimental part of the work. The experimental setup is described and flight test results are presented and discussed. Finally, Section 5 presents some concluding remarks. A preliminary version of the material presented in this paper had been accepted for presentation at the 2013 European Control Conference [23]. A video with experimental results for the proposed leader–follower strategy is available at [24].

2. Leader-following trajectory generation

The trajectory generator uses the motion of the leader to generate trajectories to be tracked by the remaining vehicles of the formation. The generation of the vertical component of the trajectory is separated from the horizontal part. We start by describing the trajectory generator for the horizontal motion, which is in fact a nonlinear control law that stabilizes, at a predefined distance vector, the position of the leader in the body frame of the virtual follower. Although, in the next section, we concentrate on a single leader–follower formation, notice that the leader may have several followers and, as discussed further ahead, the geometry of the formation is determined by the distance vectors. In addition, the leader–follower approach can be applied in cascaded form, meaning that a follower may be the leader for other vehicles, which evidences the scalability of this approach.

2.1. Problem formulation

The goal of the trajectory generator is to define a control law for a virtual follower that drives the position of the leader relative to the follower to a desired distance vector. Let $\{I\}$ denote an inertial frame, $\{L\}$ the body frame of the leader, and $\{F\}$ the body frame of the follower. The position of the origin of $\{L\}$ expressed in $\{I\}$ is given by $\mathbf{p}_L \in \mathbb{R}^2$ and the configuration of $\{F\}$ with respect to $\{I\}$ is described by an element of the Special Euclidean Group of order 2, $(\mathcal{R}, \mathbf{p}_F) = \left({}^I_F\mathbf{R}, {}^I\mathbf{p}_F\right) \in SE(2)$. The matrix $\mathcal{R}$ can be parametrized by an angle ψ, so that

$$\mathcal{R} = \begin{bmatrix} \cos\psi & -\sin\psi \\ \sin\psi & \cos\psi \end{bmatrix}. \tag{1}$$

It is assumed that the motion of the leader is known up to the second derivative $\{\mathbf{p}_L(t), \dot{\mathbf{p}}_L(t), \ddot{\mathbf{p}}_L(t)\}$, for $t \geq 0$. In what follows, time dependence is often omitted to lighten notation.

The position of leader relative to the follower can be written as

$${}^F\mathbf{p}_L = \mathcal{R}^T (\mathbf{p}_L - \mathbf{p}_F) \tag{2}$$

and the trajectory generation problem can be defined as the problem of designing a control law for the virtual follower that drives ${}^F\mathbf{p}_L$ to a desired distance vector $\mathbf{d} = [d_x \; d_y]^T$. To guarantee that the trajectory generation problem is well-defined, we introduce constraints on the motion of the virtual followers. These are actuated in forward force and torque so as to constrain their motion to the longitudinal direction.

The kinematic equations of motion can be written as

$$\dot{\mathcal{R}} = \mathcal{R}S(r) \tag{3}$$

$$\dot{\mathbf{p}}_F = \mathcal{R}[u \; 0]^T \tag{4}$$

where $u \in \mathbb{R}$ and $r \in \mathbb{R}$ are the linear and angular speeds, respectively, and $S(x)$ is a skew-symmetric matrix given by $S(x) = \begin{bmatrix} 0 & -x \\ x & 0 \end{bmatrix}$. The dynamic equations of motion are simply given by

$$\dot{u} = T \tag{5}$$

$$\dot{r} = \tau. \tag{6}$$

2.2. Controller design

Consider a position error given by

$$\mathbf{e}_1 = {}^F\mathbf{p}_L - \mathbf{d}, \tag{7}$$

with time derivative given by

$$\dot{\mathbf{e}}_1 = -S(r)\,(\mathbf{e}_1 + \mathbf{d}) + \mathcal{R}^T\dot{\mathbf{p}}_L - [u\ 0]^T, \tag{8}$$

and define a first Lyapunov candidate function as

$$V_1 = \frac{1}{2k_1}\mathbf{e}_1^T\mathbf{e}_1. \tag{9}$$

Computing the time derivative of V_1 yields

$$\begin{aligned}\dot{V}_1 &= \frac{1}{k_1}\mathbf{e}_1^T\left[-S(r)\mathbf{d} + \mathcal{R}^T\dot{\mathbf{p}}_L - [u\ 0]^T\right]\\ &= -\mathbf{e}_1^T\boldsymbol{\sigma}(\mathbf{e}_1)\\ &\quad + \mathbf{e}_1^T\left[\boldsymbol{\sigma}(\mathbf{e}_1) + \frac{1}{k_1}\left(-S(r)\mathbf{d} + \mathcal{R}^T\dot{\mathbf{p}}_L - [u\ 0]^T\right)\right]\end{aligned} \tag{10}$$

where we have used the map $\boldsymbol{\sigma} : \mathbb{R}^2 \mapsto \mathbb{R}^2$ to denote a saturation function applied element-wise and given by

$$\boldsymbol{\sigma}(x) = [\sigma_K(x_1)\ \sigma_K(x_2)]^T \tag{11}$$

and σ_K is a K-saturation function defined as follows.

Definition 1. A K-saturation function is a smooth increasing function $\sigma_K : \mathbb{R} \mapsto \mathbb{R}$ that satisfies the following properties:

1. $\sigma_K(0) = 0$,
2. $s\sigma_K(s) > 0$ for all $s \neq 0$,
3. $\lim_{s\to\pm\infty}\sigma_K(s) = \pm K$ for some $K > 0$.

Following the backstepping procedure, a new error is defined

$$\mathbf{e}_2 = \boldsymbol{\sigma}(\mathbf{e}_1) + \frac{1}{k_1}\left(-S(r)\mathbf{d} + \mathcal{R}^T\dot{\mathbf{p}}_L - [u\ 0]^T\right) \tag{12}$$

and the Lyapunov candidate function extended to include it, so that

$$V_2 = V_1 + \frac{1}{2k_2}\mathbf{e}_2^T\mathbf{e}_2. \tag{13}$$

Assuming the presence of constant disturbances on the actuations T and τ, the expression for $\dot{\mathbf{e}}_2$ can be written as

$$\dot{\mathbf{e}}_2 = \dot{\boldsymbol{\sigma}}(\mathbf{e}_1) + \frac{1}{k_1}\left(\boldsymbol{\delta} - \boldsymbol{\Gamma}\boldsymbol{\mu}\right) + \mathbf{b} \tag{14}$$

where

$$\boldsymbol{\Gamma} = \begin{bmatrix}1 & -d_y\\ 0 & d_x\end{bmatrix}, \quad \boldsymbol{\mu} = \begin{bmatrix}T\\ \tau\end{bmatrix}, \quad \boldsymbol{\delta} = -S(r)\mathcal{R}^T\dot{\mathbf{p}}_L + \mathcal{R}^T\ddot{\mathbf{p}}_L, \tag{15}$$

and $\mathbf{b} \in \mathbb{R}^2$ is an unknown constant. The time derivative of V_2 is then given by

$$\dot{V}_2 = -\mathbf{e}_1^T\boldsymbol{\sigma}(\mathbf{e}_1) + \mathbf{e}_1^T\mathbf{e}_2 + \frac{\mathbf{e}_2^T}{k_1k_2}\left(k_1\dot{\boldsymbol{\sigma}}(\mathbf{e}_1) + \boldsymbol{\delta} - \boldsymbol{\Gamma}\boldsymbol{\mu} + k_1\mathbf{b}\right). \tag{16}$$

Notice that $\boldsymbol{\Gamma}$ is invertible, provided that $d_x \neq 0$.

In order to achieve convergence of the tracking errors to zero and reject the constant disturbance $\mathbf{b}$, we introduce the integral state $\boldsymbol{\xi}$ with dynamics

$$\dot{\boldsymbol{\xi}} = \mathbf{e}_2 \tag{17}$$

and a new Lyapunov candidate function given by

$$V_3 = V_2 + \frac{k_3}{2k_2}\left(\boldsymbol{\xi} - \tfrac{1}{k_3}\mathbf{b}\right)^T\left(\boldsymbol{\xi} - \tfrac{1}{k_3}\mathbf{b}\right), \tag{18}$$

whose time derivative is given by

$$\begin{aligned}\dot{V}_3 &= \dot{V}_2 + \frac{k_3}{k_2}\left(\boldsymbol{\xi} - \tfrac{1}{k_3}\mathbf{b}\right)^T\mathbf{e}_2\\ &= -\mathbf{e}_1^T\boldsymbol{\sigma}(\mathbf{e}_1) + \mathbf{e}_1^T\mathbf{e}_2 + \frac{\mathbf{e}_2^T}{k_1k_2}\left(k_1\dot{\boldsymbol{\sigma}}(\mathbf{e}_1) + \boldsymbol{\delta} + k_1k_3\boldsymbol{\xi} - \boldsymbol{\Gamma}\boldsymbol{\mu}\right).\end{aligned} \tag{19}$$

At this point we can define a control law for $\boldsymbol{\mu}$ that renders $\dot{V}_3$ negative semi-definite and globally asymptotically stabilizes the origin of the error system. This result is stated formally in the following Theorem.

Theorem 1. *Consider the simplified vehicle model described by (3)–(6) and the error system with state given by* $\mathbf{e}_1$ *(7),* $\mathbf{e}_2$ *(12), and* $\boldsymbol{\xi}' = \boldsymbol{\xi} - \frac{1}{k_3}\mathbf{b}$*. The control law*

$$\boldsymbol{\mu} = \Gamma^{-1}\left(\boldsymbol{\delta} + k_1\dot{\boldsymbol{\sigma}}(\mathbf{e}_1) + k_1k_2\mathbf{e}_2 + k_1k_3\boldsymbol{\xi}\right), \tag{20}$$

with positive gains k_1*,* k_2*, and* k_3*, renders the origin of the error system globally asymptotically stable.*

Proof. Using the control law (20), the overall closed-loop system can be written as

$$\dot{\mathbf{e}}_1 = -S(r)\mathbf{e}_1 - k_1\boldsymbol{\sigma}(\mathbf{e}_1) + k_1\mathbf{e}_2, \tag{21}$$

$$\dot{\mathbf{e}}_2 = -k_2\mathbf{e}_2 - k_3\boldsymbol{\xi}', \tag{22}$$

$$\dot{\boldsymbol{\xi}}' = \mathbf{e}_2. \tag{23}$$

By noting that the subsystem (22)–(23) is a double-integrator system regulated by negative feedback of its states, we can immediately conclude that ($\mathbf{e}_2 = 0, \boldsymbol{\xi} = 0$) is globally asymptotically stable. In particular, the Lyapunov function

$$W = \frac{1}{2}\boldsymbol{\xi}'^T\boldsymbol{\xi}' + \frac{1}{k_3}\mathbf{e}_2^T\mathbf{e}_2 + \frac{1}{2}\boldsymbol{\epsilon}^T\boldsymbol{\epsilon},$$

where $\boldsymbol{\epsilon} = \frac{k_2}{k_3}\mathbf{e}_2 + \boldsymbol{\xi}'$, has a negative definite time derivative given by $\dot{W} = -\frac{k_2}{k_3}\mathbf{e}_2^T\mathbf{e}_2 - k_2\boldsymbol{\epsilon}^T\boldsymbol{\epsilon}$.

To analyze the stability of (21)–(23), note that substituting (20) in (16) yields

$$\begin{aligned}\dot{V}_3 &= -\mathbf{e}_1^T\boldsymbol{\sigma}(\mathbf{e}_1) + \mathbf{e}_1^T\mathbf{e}_2 - \mathbf{e}_2^T\mathbf{e}_2\\ &\leq -\|\mathbf{e}_1\|\left(\tfrac{\sqrt{2}}{2}\|\boldsymbol{\sigma}(\mathbf{e}_1)\| - \|\mathbf{e}_2\|\right) - \|\mathbf{e}_2\|^2.\end{aligned}$$

If $\|\mathbf{e}_2\| \leq \frac{\sqrt{2}}{2}K$, $\dot{V}_3$ can only have a positive term if $\frac{\sqrt{2}}{2}\|\boldsymbol{\sigma}(\mathbf{e}_1)\| - \|\mathbf{e}_2\| < 0$ or equivalently if $\|\boldsymbol{\sigma}(\mathbf{e}_1)\| < \sqrt{2}\|\mathbf{e}_2\| \leq K$. However, in this case, $\|\boldsymbol{\sigma}(\mathbf{e}_1)\| = \|\mathbf{e}_1\|$, meaning that $\dot{V}_3 \leq 0$ for $\|\mathbf{e}_2\| \leq \frac{\sqrt{2}}{2}K$. Since there exists a finite time T, such that $\|\mathbf{e}_2(t)\| \leq \frac{\sqrt{2}}{2}K$ for $t > T$, then $\dot{V}_3$ will become negative semi-definite in finite time and $V_3 + W$ will have a negative definite time derivative, implying that the origin is globally asymptotically stable. □

2.3. Inner dynamics analysis

Having a stabilized error system does not imply that the intrinsic variables of the vehicle are all stabilized. For a given leader's position and a given $\mathbf{d}$ there are infinite solutions depending on the follower's attitude that yield null position error, which indicates the existence of a zero dynamics, whose stability needs to be analyzed. Towards that end, consider the limit condition when the errors have converged to zero. In that situation the following relation is verified:

$$\begin{bmatrix}u\\ \dot{\psi}\end{bmatrix} = \boldsymbol{\Gamma}^{-1}\mathcal{R}^T\dot{\mathbf{p}}_L. \tag{24}$$

Let $\dot{\mathbf{p}}_L$ be given by

$$\dot{\mathbf{p}}_L = V_L \begin{bmatrix} \cos\psi_L \\ \sin\psi_L \end{bmatrix}, \tag{25}$$

where V_L and ψ_L are continuous functions of time representing the norm and direction of the leader's velocity, respectively. Using these definitions, (24) can be rearranged into the form

$$\begin{bmatrix} u \\ \dot{\psi} \end{bmatrix} = \begin{bmatrix} V_L \cos(\psi_L - \psi) + \dfrac{V_L d_y}{d_x} \sin(\psi_L - \psi) \\ \dfrac{V_L}{d_x} \sin(\psi_L - \psi) \end{bmatrix}. \tag{26}$$

Applying the change of variables $\psi_r = \psi - \psi_L$, the zero dynamics can be written as

$$\dot{\psi}_r = -\frac{V_L}{d_x}(\sin\psi_r + d_x\kappa_L), \tag{27}$$

where $\kappa_L = r_L/V_L$ is the curvature of the leader's path. It is worth noting that the second equation does not depend on d_y.

The analysis that follows is divided into two cases: (a) trajectories with $\dot{\kappa}_L = 0$; and (b) trajectories with $\dot{\kappa}_L \neq 0$.

For $\dot{\kappa}_L = 0$. Trajectories with $\dot{\kappa}_L = 0$ can be either a circumference ($\kappa_L \neq 0$), or a straight line ($\kappa_L = 0$). To analyze the stability of (27) for these types of trajectories, consider the candidate Lyapunov function

$$V_\psi = \frac{1}{2}(\sin\psi_r + d_x\kappa_L)^2, \tag{28}$$

whose time derivative is given by

$$\dot{V}_\psi = -2\frac{V_L}{d_x}\cos\psi_r\, V_\psi. \tag{29}$$

For simplicity, consider the case when $d_x > 0$ (a similar reasoning can be applied when $d_x < 0$). From (29), it follows that $\dot{V}_\psi$ is zero for $\psi_r = \pm\pi/2$ and for $\sin\psi_r = -d_x\kappa_L$, and negative definite whenever $\cos\psi_r > 0$. Analyzing (29), it can be shown that, if $|d_x\kappa_L| \leq 1$ then $\psi_r = -\arcsin(d_x\kappa_L)$ is an asymptotically stable equilibrium point, whereas $\psi_r = \pi - \arcsin(d_x\kappa_L)$ is unstable. Also, if $|d_x\kappa_L| > 1$ then $\lim_{t\to+\infty} |\psi_r| = +\infty$. From (26), it follows immediately that $|\dot{\psi}| \leq |\frac{V_L}{d_x}|$ and therefore $|\dot{\psi}| < |\dot{\psi}_L|$, meaning that the follower can never reach the angular velocity of the leader and the angular distance ψ_r diverges. Notice, however, that the condition $|d_x\kappa_L| \leq 1$ imposes no constraint on the curvature of the follower, since we can use d_y to select an arbitrary curvature.

For $\dot{\kappa}_L \neq 0$. When the trajectory being tracked has a time-varying curvature, the analysis is more involved and asymptotic stability for the general case is difficult to assess. Nevertheless, it is possible to prove the boundedness of ψ_r, provided that $|d_x\kappa_L(t)| < 1$, for all time. The following proposition is provided for $d_x > 0$. A similar reasoning can be applied for $d_x < 0$.

Lemma 2. *Assume that $d_x > 0$ and $|d_x\kappa_L(t)| < \varepsilon < 1$, for all $t \geq 0$. Let Ω_1 and Ω_2 denote the sets $\Omega_1 = \{\psi_r : |\sin\psi_r| \leq \varepsilon, \cos\psi_r > 0\}$ and $\Omega_2 = \Omega_1 \cup \{\psi_r : |\sin\psi_r| \geq \varepsilon\}$, respectively. Then $\psi_r(t)$ is bounded, Ω_1 and Ω_2 are positively invariant, and any solution starting in Ω_2 will enter Ω_1 in finite time.*

Proof. Consider the Lyapunov function candidate

$$W_\psi = 1 - \cos\psi_r. \tag{30}$$

Computing the time derivative of W_ψ, it can be shown that

$$\dot{W}_\psi < -\frac{V_L}{d_x}|\sin\psi_r|(|\sin\psi_r| - \varepsilon),$$

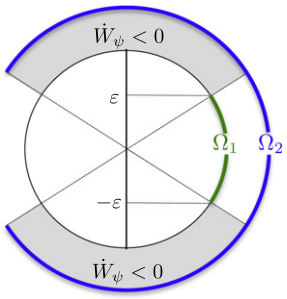

Fig. 1. Graphical representation of the positively invariant sets Ω_1 and Ω_2.

which is negative definite for $|\sin\psi_r| \geq \varepsilon$. Hence, the sets Ω_1 and Ω_2, shown in Fig. 1, are positively invariant and any solution starting in Ω_2 will enter Ω_1 in finite time. Solutions starting outside the set Ω_2 cannot grow unbounded, since to do so they would have to enter Ω_2, in which case the above applies. Thus, provided that $\varepsilon < 1$, ψ_r is bounded irrespective of its initial value. □

Lemma 2 shows that if a bound on the curvature of the leader's path κ_L is known, d_x can be chosen so that $|d_x\kappa_L(t)| < 1$ to guarantee that the angular distance between the leader and the follower given by ψ_r also remains within known bounds. This boundedness property (which is a direct consequence of the kinematic constraints imposed on the motion of the virtual follower) together with the stability in position guarantees that the generated trajectory is "well-behaved" and simultaneously richer in terms of curvature variation than a simple offset version of the leader's trajectory.

The bound $|d_x\kappa_L(t)| < 1$ does not, however, prevent inversions in the directions of motion of the virtual followers from occurring. Such a behavior can affect the performance of the real vehicles while tracking the generated trajectories and thus it is of interest to avoid it. Rewriting the first part of (26) as

$$u\frac{d_x}{V_L} = d_x\cos\psi_r - d_y\sin\psi_r,$$

and assuming once again that $d_x > 0$, it can be shown that u will remain positive as long as

$$d_y\sin\psi_r > d_x\cos\psi_r$$

holds. Combining this condition with Lemma 2, we can obtain a bound for the initial value of the angular distance $\psi_r(0)$, which guarantees that no inversion will occur. More specifically, if

$$\arcsin|d_x\kappa_L(t)| < \operatorname{atan2}(d_x, |d_y|) \tag{31}$$

$u(0) > 0$, and $\psi_r(0) \in \Omega_1$, then $u(t) > 0$, for all $t > 0$.

The simulation results presented in the following section illustrate the type and richness of the trajectories that can be generated using the virtual vehicle model (3)–(6) in closed-loop with the control law defined in (20).

2.4. Simulation results

Consider the case where two vehicles are supposed to follow a leader describing a lemniscate trajectory given by

$$\mathbf{p}_L(t) = \begin{bmatrix} 2\cos(0.25t) \\ \sin(0.5t) \end{bmatrix}. \tag{32}$$

The desired distance for follower 1 is set to $\mathbf{d}_1 = [0.35\ 0.35]^T$ and its initial state to $\mathbf{p}_{F1}(0) = [3\ 3]^T$, $u_{F1}(0) = 0.5$, $r_{F1}(0) = -0.5$, $\psi_{F1}(0) = 3\pi/2$. For follower 2, we select $\mathbf{d}_2 = [0.35\ -0.35]^T$, and set $\mathbf{p}_{F2}(0) = [3\ 1]^T$, $u_{F2}(0) = 0$, $r_{F2}(0)$

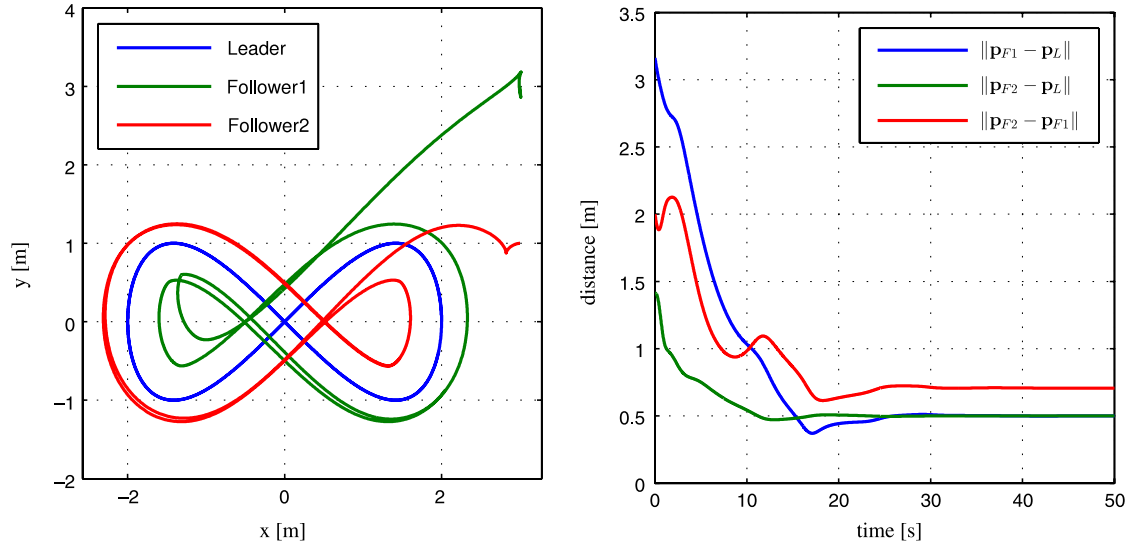

(a) Position. (b) Distance between virtual vehicles.

Fig. 2. Position and distance between leader and virtual followers.

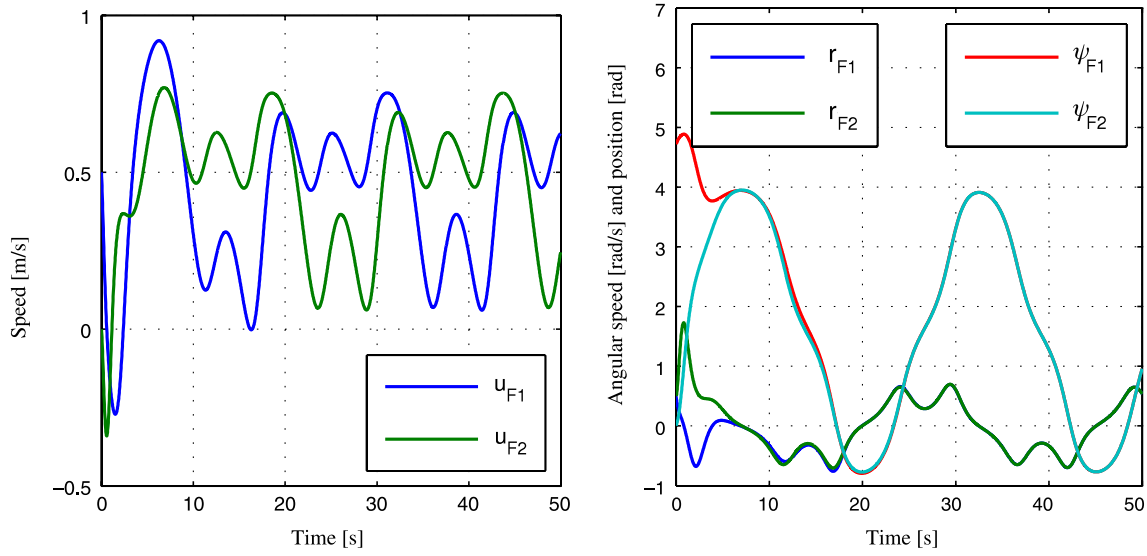

(a) Linear speed. (b) Angular speed and angular position.

Fig. 3. States of the virtual followers.

$= 0.5$, $\psi_{F2}(0) = 0$. The controller parameters are $k_1 = 0.2$, $k_2 = 2$, $k_3 = 0$, and $K = 5$.

Although the trajectories of both followers are different (see Fig. 2(a)), their angular velocity and angular position converge to the same values (see Fig. 3(b)). This is in agreement with the analysis made in Section 2.3, where it was concluded that these variables do not depend on d_y, which in this case is the only differing parameter.

Fig. 2(b) shows that the distance between followers and between these and the leader converge to fixed values. The latter is a direct implication of the asymptotic stability of the error system, as shown in Fig. 4. The former, the distance between followers, is a result of the fact that, at the equilibrium, the follower's states u, r and ψ do not depend on d_y. The value to which this distance converges is equal to the sum of the followers' distances, in this case $0.35 + 0.35 = 0.7$ m. These results indicate that a formation where all the followers have the same value of d_x converges to a rigid formation. Future work will focus on deriving a formal proof of convergence.

2.5. Three-dimensional trajectories

So far only two-dimensional motion has been considered. However, to generate trajectories for quadrotors it is necessary to consider three-dimensional motion. Instead of deriving a law for the entire state space, a separate control law is designed to drive the vertical coordinate of each virtual follower to a desired distance to the leader. Consider that the desired vectorial distance $\mathbf{d}$ is extended to include a third component d_z and let e_z be the vertical position error given by

$$e_z = p_{Lz} - p_{Fz} - d_z. \tag{33}$$

A simple control law that stabilizes e_z is given by

$$\ddot{p}_{Fz} = \sigma_K(\ddot{p}_{Lz}) + \sigma_K(k_{z1}e_z + k_{z2}\dot{e}_z). \tag{34}$$

This saturation is introduced to protect the followers from any unexpected acceleration of the leader. The control law asymptotically stabilizes e_z at the origin, provided that $|\ddot{p}_{Lz}| < K$ holds.

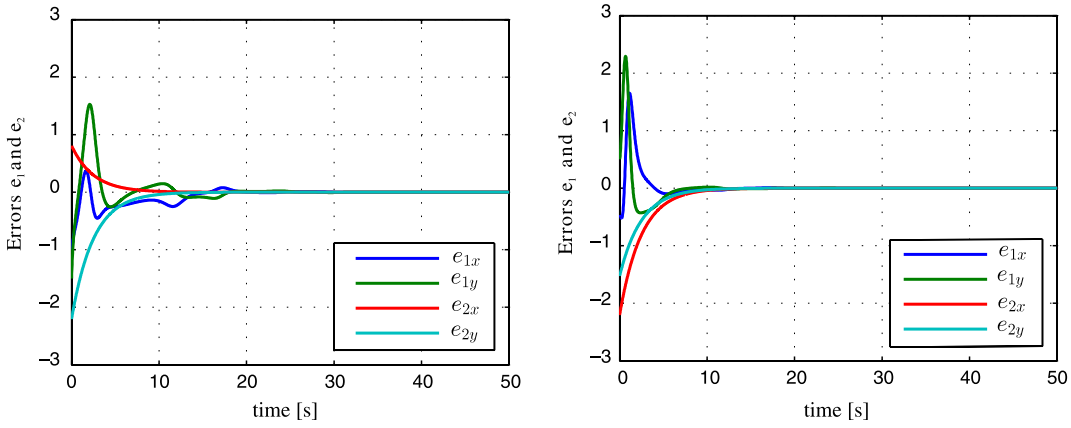

(a) Virtual follower 1. (b) Virtual follower 2.

Fig. 4. Time evolution of the position and velocity errors.

2.6. Planner initialization

As noted in Section 2.3, inversions in the directions of motion of the virtual followers can affect the performance of the real vehicles tracking the trajectories. In order to prevent this behavior, the trajectory described by the leader and the desired configurations of the virtual followers have to verify (31). To this end, the virtual followers are initialized with $\psi_r(0) = 0$ and zero error, with respect to the reference trajectory of the leader, while the real vehicles are converging to their formation positions.

Until both the leader and follower vehicles approach the initial reference and virtual followers, respectively, the generator is kept turned off. Once that happens the generator is turned on and the leader starts tracking the reference trajectory. The choice to initially place the virtual followers with respect to the reference trajectory of the leader allows for faster formation initialization, and guarantees that, when the generator is started, the actual values of the angles ψ_r verify the aforementioned bounds.

The tracking is triggered when the components of the position error of each vehicle verify the condition $e_i = \|\mathbf{p}_{Fi} - \mathbf{p}_{vFi}(0)\| < e_{\max}$, i.e.,

$$trigger = (e_L < e_{\max}) \wedge (e_1 < e_{\max}) \wedge \cdots \wedge (e_n < e_{\max}) \tag{35}$$

where $e_{\max}$ is a configurable parameter that defines the threshold used to start the tracking.

3. Quadrotors in formation

3.1. Quadrotor model

The quadrotor vehicles are modeled as rigid bodies actuated in force and torque. Consider a fixed inertial frame $\{I\}$ and frames $\{B\}$ attached to each vehicle's center of mass. The configuration of the body frame $\{B\}$ with respect to $\{I\}$ can be viewed as an element of the Special Euclidean group, $(\mathbf{R}, \mathbf{p}) = ({}^I_B\mathbf{R}, {}^I\mathbf{p}_B) \in SE(3)$. The kinematic and dynamic equations of motion for the rigid body can be written as

$$\dot{\mathbf{R}} = \mathbf{R}S(\boldsymbol{\omega}) \tag{36}$$

$$\dot{\mathbf{p}} = \mathbf{R}\mathbf{v} \tag{37}$$

$$\dot{\mathbf{v}} = -S(\boldsymbol{\omega})\mathbf{v} + \frac{1}{m}\mathbf{f}_{\text{ext}} \tag{38}$$

$$\dot{\boldsymbol{\omega}} = -\mathbf{J}^{-1}S(\boldsymbol{\omega})\mathbf{J}\boldsymbol{\omega} + \mathbf{J}^{-1}\mathbf{m}_{\text{ext}}. \tag{39}$$

In the foregoing equations, $\boldsymbol{\omega} \in \mathbb{R}^3$ and $\mathbf{v} \in \mathbb{R}^3$ denote the angular and linear velocities and $\mathbf{f}_{\text{ext}} \in \mathbb{R}^3$ and $\mathbf{m}_{\text{ext}} \in \mathbb{R}^3$ represent the external forces and moments acting on the vehicle, respectively, all expressed in the body frame. $S(\cdot)$ is a skew-symmetric matrix of its argument verifying $S(\mathbf{a})\mathbf{b} = \mathbf{a} \times \mathbf{b}$, where $\times$ denotes the cross-product operator and $\mathbf{a}$ and $\mathbf{b} \in \mathbb{R}^3$. Lastly, m is the mass of the vehicle and $\mathbf{J}$ the tensor of inertia.

The most commonly adopted dynamic model for quadrotors (e.g. [25]) considers that torques can be generated in any direction and that the only actuation force is the thrust T, aligned with the body's vertical axis. The external force is then given by

$$\mathbf{f}_{\text{ext}} = -T\mathbf{u}_3 + mg\mathbf{R}^T\mathbf{u}_3, \tag{40}$$

where $\mathbf{u}_3 = [0\ 0\ 1]^T$ and g is the gravitational acceleration. As the vehicle has full torque actuation, the input transformation

$$\mathbf{m}_{\text{ext}} = \mathbf{J}\boldsymbol{\tau} + S(\boldsymbol{\omega})\mathbf{J}\boldsymbol{\omega} \tag{41}$$

can be used to reduce Eq. (39) to an integrator form

$$\dot{\boldsymbol{\omega}} = \boldsymbol{\tau}. \tag{42}$$

From (40) and (41), we conclude that the quadrotor is underactuated with only four actuation variables for six degrees of freedom.

3.2. Quadrotor trajectory tracking controller

Let the desired trajectory be given by $\mathbf{p}_d(t) \in \mathbb{R}^3$, a function of time at least of class C^4. In the sequel, time dependence will be omitted to lighten notation. In this section, we derive a control law for trajectory tracking that builds on the principle of assigning an appropriate thrust and using the torque actuation to ensure convergence to an appropriate thrust direction.

Consider the position error

$$\mathbf{e}_1 = \mathbf{p} - \mathbf{p}_d \tag{43}$$

and the velocity error

$$\mathbf{e}_2 = \dot{\mathbf{e}}_1 = \mathbf{R}\mathbf{v} - \dot{\mathbf{p}}_d, \tag{44}$$

with time derivative given by

$$\dot{\mathbf{e}}_2 = -\frac{T}{m}\mathbf{r}_3 + g\mathbf{u}_3 - \ddot{\mathbf{p}}_d,$$

where $\mathbf{r}_3 = \mathbf{R}\mathbf{u}_3$. The error system can be rewritten as a double-integrator system driven by a constrained input to take the form

$$\dot{\mathbf{e}}_1 = \mathbf{e}_2 \tag{45}$$

$$\dot{\mathbf{e}}_2 = \mathbf{u}^* - \frac{T}{m}\mathbf{r}_3 + \frac{T_d}{m}\mathbf{r}_{3d}, \tag{46}$$

where the desired thrust T_d and desired thrust direction $\mathbf{r}_{3d}$ are given by

$$T_d = m\|g\mathbf{u}_3 - \ddot{\mathbf{p}}_d + \mathbf{u}^*\|, \tag{47}$$

$$\mathbf{r}_{3d} = \frac{g\mathbf{u}_3 - \ddot{\mathbf{p}}_d + \mathbf{u}^*}{\|g\mathbf{u}_3 - \ddot{\mathbf{p}}_d + \mathbf{u}^*\|}, \tag{48}$$

respectively, and $\mathbf{u}^* \in \mathbb{R}^3$ denotes the desired input vector, which would be applied if full actuation were available.

Given that $\mathbf{r}_{3d}$ is not well-defined when $T_d = 0$, it is of interest to define a desired input $\mathbf{u}^*$ that simultaneously stabilizes the double-integrator dynamics and guarantees that T_d does not cross the origin. For that purpose, we consider the saturated PD controller given by

$$\mathbf{u}^* = -\boldsymbol{\sigma}(k_1\mathbf{e}_1 + k_2\mathbf{e}_2), \tag{49}$$

where $\boldsymbol{\sigma} : \mathbb{R}^3 \mapsto \mathbb{R}^3$ is a saturation function applied element-wise and defined such that

$$\boldsymbol{\sigma}(\mathbf{x}) = \begin{bmatrix}\sigma_K(x_1) & \sigma_K(x_2) & \sigma_K(x_3)\end{bmatrix}^T. \tag{50}$$

To ensure that T_d remains positive, we assume that the limit of the saturation function is chosen such that

$$\|\ddot{\mathbf{p}}_d - \mathbf{u}^*\| < g. \tag{51}$$

It is well known that the saturated control law of the form given in (49) globally asymptotically stabilizes a double-integrator system [26]. In this paper, we present an alternative proof of this result that provides a strict Lyapunov function, in the sense that the time derivative along the closed-loop trajectories of the system is strictly negative definite instead of just negative semi-definite.

Lemma 3. *Consider the scalar double-integrator system given by*

$$\dot{x}_1 = x_2 \tag{52}$$

$$\dot{x}_2 = u \tag{53}$$

and let $u = -k_1x_1 - k_2x_2$ be an asymptotically stabilizing controller. Then, the closed-loop system that results from the feedback interconnection of (52)–(53) and the controller

$$u = -\sigma_K(k_1x_1 + k_2x_2) \tag{54}$$

has a globally asymptotically stable equilibrium point at the origin.

Proof. Consider the candidate Lyapunov function V_0 given by

$$V_0(x_1, x_2) = \frac{1}{2}\begin{bmatrix}\sigma_K(s) & x_2\end{bmatrix}\mathbf{P}_0\begin{bmatrix}\sigma_K(s)\\ x_2\end{bmatrix} + \int_0^s \sigma_K(\xi)d\xi \tag{55}$$

where $s = k_1x_1 + k_2x_2$ and $\mathbf{P}_0$ is positive definite. It can be shown that V_0 is positive definite and radially unbounded. Let $\mathbf{P}_0$ be given by

$$\mathbf{P}_0 = \begin{bmatrix}a & -b\\ -b & c\end{bmatrix}. \tag{56}$$

Then, $\dot{V}_0$ can be written as

$$\dot{V}_0 = -\begin{bmatrix}\sigma_K(s) & x_2\end{bmatrix}\mathbf{Q}_0\begin{bmatrix}\sigma_K(s)\\ x_2\end{bmatrix},$$

where $\mathbf{Q}_0$ is given by

$$\mathbf{Q}_0 = \begin{bmatrix}k_2 - b & \frac{1}{2}(c - k_1)\\ \frac{1}{2}(c - k_1) & 0\end{bmatrix} + \frac{\partial\sigma_K(s)}{\partial s}\begin{bmatrix}k_2a & -\frac{1}{2}(k_1a + k_2b)\\ -\frac{1}{2}(k_1a + k_2b) & k_1b\end{bmatrix}.$$

For any $k_1 > 0$ and $k_2 > 0$ and taking into account that $\frac{\partial\sigma_K(s)}{\partial s} > 0$ according to Definition 1, we can show that choosing a, b, and c such that $\mathbf{P}_0 > 0$, $k_1 = c$, and $k_2 = \frac{ac}{b}$ yields $\mathbf{Q}_0 > 0$. It follows that the closed-loop system has a globally asymptotically stable equilibrium point at the origin. □

Going back to the original error system (45)–(46), consider the following control law for the thrust T:

$$T = \mathbf{r}_{3d}^T\mathbf{r}_3T_d, \tag{57}$$

which results from the projection of the desired thrust vector $T_d\mathbf{r}_{3d}$ on the current body z-axis given by $\mathbf{r}_3$. Then, $\dot{\mathbf{e}}_2$ can be rewritten as

$$\dot{\mathbf{e}}_2 = \mathbf{u}^* - \frac{T_d}{m}\mathbf{S}(\mathbf{r}_3)^2\mathbf{r}_{3d},$$

where the second term encodes the angular distance between the directions $\mathbf{r}_3$ and $\mathbf{r}_{3d}$. Using Lemma 3, we can define the Lyapunov function

$$V_\sigma(\mathbf{e}_1, \mathbf{e}_2) = \frac{1}{2}\begin{bmatrix}\boldsymbol{\sigma}(\mathbf{s})^T & \mathbf{e}_2^T\end{bmatrix}\mathbf{P}\begin{bmatrix}\boldsymbol{\sigma}(\mathbf{s})\\ \mathbf{e}_2\end{bmatrix} + \sum_i \int_0^{\mathbf{u}_i^T\mathbf{s}} \sigma_K(\xi)d\xi, \tag{58}$$

where $\mathbf{s} = k_1\mathbf{e}_1 + k_2\mathbf{e}_2$ and $\mathbf{P}$ is the block matrix version of $\mathbf{P}_0$. Computing the time derivative, we obtain

$$\dot{V}_\sigma = -\begin{bmatrix}\boldsymbol{\sigma}(\mathbf{s})^T & \mathbf{e}_2^T\end{bmatrix}\mathbf{Q}\begin{bmatrix}\boldsymbol{\sigma}(\mathbf{s})\\ \mathbf{e}_2\end{bmatrix} - \frac{T_d}{m}\mathbf{r}_{3d}^T\mathbf{S}(\mathbf{r_3})^2\boldsymbol{\delta}(\mathbf{e}_1, \mathbf{e}_2), \tag{59}$$

where, similarly to $\mathbf{P}$, $\mathbf{Q}$ is the block matrix version of $\mathbf{Q}_0$ and

$$\boldsymbol{\delta}(\mathbf{e}_1, \mathbf{e}_2) = k_2\frac{\partial\boldsymbol{\sigma}(\mathbf{s})}{\partial\mathbf{s}}(a\boldsymbol{\sigma}(\mathbf{s}) - b\mathbf{e}_2) + (k_2 - b)\boldsymbol{\sigma}(\mathbf{s}) + c\mathbf{e}_2. \tag{60}$$

To drive $\mathbf{r}_3$ to $\mathbf{r}_{3d}$, we apply the backstepping technique based on the attitude error, which can be written in vector form as

$$\mathbf{e}_3 = \mathbf{r}_3 - \mathbf{r}_{3d} \tag{61}$$

or as an angular error given by

$$\cos\theta_3 = 1 - \frac{1}{2}\mathbf{e}_3^T\mathbf{e}_3 = \mathbf{r}_3^T\mathbf{r}_{3d} \tag{62}$$

and consider the candidate Lyapunov function

$$V_3 = V_\sigma + \frac{1}{2}\mathbf{e}_3^T\mathbf{e}_3 = V_\sigma + 1 - \cos\theta_3. \tag{63}$$

Computing the time derivative of V_3 yields

$$\begin{aligned}\dot{V}_3 &= \dot{V}_\sigma + \mathbf{r}_{3d}^T\mathbf{R}\mathbf{S}(\mathbf{u}_3)\left(\boldsymbol{\omega} - \mathbf{R}^T\mathbf{S}(\mathbf{r}_{3d})\dot{\mathbf{r}}_{3d}\right)\\ &= -W_3(\mathbf{e}_1, \mathbf{e}_2, \mathbf{r}_3, \mathbf{r}_{3d}) + \mathbf{r}_{3d}^T\mathbf{R}S(\mathbf{u}_3)(\boldsymbol{\omega} - \boldsymbol{\omega}_d),\end{aligned} \tag{64}$$

where

$$\begin{aligned}W_3(\mathbf{e}_1, \mathbf{e}_2, \mathbf{r}_3, \mathbf{r}_{3d}) &= \begin{bmatrix}\boldsymbol{\sigma}(\mathbf{s})^T & \mathbf{e}_2^T\end{bmatrix}\mathbf{Q}\begin{bmatrix}\boldsymbol{\sigma}(\mathbf{s})\\ \mathbf{e}_2\end{bmatrix}\\ &\quad + k_3\mathbf{r}_{3d}^T\mathbf{S}(\mathbf{r}_3)^T\mathbf{S}(\mathbf{r}_3)\mathbf{r}_{3d}\end{aligned} \tag{65}$$

and

$$\boldsymbol{\omega}_d = \mathbf{R}^T\mathbf{S}(\mathbf{r}_{3d})\dot{\mathbf{r}}_{3d} + S(\mathbf{u}_3)\mathbf{R}^T\left(k_3\mathbf{r}_{3d} + \frac{T_d}{m}\boldsymbol{\delta}(\mathbf{e}_1, \mathbf{e}_2)\right). \tag{66}$$

To obtain a control law in torque, we apply once again the backstepping procedure and define the angular velocity error

$$\mathbf{e}_4 = S(\mathbf{u}_3)(\boldsymbol{\omega} - \boldsymbol{\omega}_d), \tag{67}$$

and the candidate Lyapunov function

$$V_4 = V_3 + \frac{1}{2}\mathbf{e}_4^T\mathbf{e}_4. \tag{68}$$

Noting that the time derivative of V_4 can be written as

$$\dot{V}_4 = -W_3(\mathbf{e}_1, \mathbf{e}_2, \mathbf{r}_3, \mathbf{r}_{3d}) + \mathbf{e}_4^T S(\mathbf{u}_3)(\boldsymbol{\tau} - \dot{\boldsymbol{\omega}}_d - S(\mathbf{u}_3)\mathbf{R}^T\mathbf{r}_{3d}), \quad (69)$$

we can define a control law for the torque $\boldsymbol{\tau}$ that renders a negative semi-definite $\dot{V}_4$ and ensures global asymptotic convergence of the trajectory tracking errors to zero. The following Theorem states formally this result.

Theorem 4. *Let the quadrotor dynamic model be described by (36)–(39), $\mathbf{p}_d(t) \in C^4$ be the desired trajectory, and consider the error coordinates $\mathbf{e}_1, \mathbf{e}_2, \mathbf{e}_3$, and $\mathbf{e}_4$, given by (43), (44), (61) and (67), respectively. For any bounded $\boldsymbol{\tau}_z(t) \in C^1$, the closed-loop system that results from applying the control laws (57) and*

$$\boldsymbol{\tau} = S(\mathbf{u}_3)(k_4\mathbf{e}_4 + \dot{\boldsymbol{\omega}}_d + S(\mathbf{u}_3)\mathbf{R}^T\mathbf{r}_{3d}) + \boldsymbol{\tau}_z\mathbf{u}_3 \quad (70)$$

achieves global trajectory tracking and ensures convergence of the errors $\mathbf{e}_1, \mathbf{e}_2$, and $\mathbf{e}_4$ to zero, for any initial condition. In addition, θ_3 converges to either 0 or π and the desired equilibrium point $(\mathbf{e}_1, \mathbf{e}_2, \theta_3, \mathbf{e}_4) = (\mathbf{0}, \mathbf{0}, 0, \mathbf{0})$ is uniformly asymptotically stable.

Proof. Substituting $\boldsymbol{\tau}$ into $\dot{V}_4$ yields

$$\dot{V}_4 = -\begin{bmatrix}\boldsymbol{\sigma}(\mathbf{s})^T & \mathbf{e}_2^T\end{bmatrix}\mathbf{Q}\begin{bmatrix}\boldsymbol{\sigma}(\mathbf{s}) \\ \mathbf{e}_2\end{bmatrix} - k_3\mathbf{r}_{3d}^T\mathbf{S}(\mathbf{r}_3)^T\mathbf{S}(\mathbf{r}_3)\mathbf{r}_{3d} - k_4\mathbf{e}_4^T\mathbf{e}_4, \quad (71)$$

which is negative semi-definite and zero-valued in the set $\{\mathbf{e}_1 = \mathbf{0}, \mathbf{e}_2 = \mathbf{0}, \mathbf{r}_3 = \pm\mathbf{r}_{3d}, \mathbf{e}_4 = \mathbf{0}\}$. Since the quadrotor error dynamics are non-autonomous, we resort to Barbalat's Lemma to show that $\dot{V}_4$ converges to zero. From the unboundedness of V_4 with respect to $\mathbf{e}_1, \mathbf{e}_2$, and $\mathbf{e}_4$ and observing that $\dot{V}_4$ is negative semi-definite, we conclude that $\mathbf{e}_1, \mathbf{e}_2$, and $\mathbf{e}_4$ are bounded. Given that $\mathbf{e}_3$ evolves on a compact set, and the external inputs $\mathbf{p}_d^{(4)}$ and $\boldsymbol{\omega}_z$ are bounded, $\ddot{V}_4$ is bounded and, consequently $\dot{V}_4$ is uniformly continuous. We can therefore apply Barbalat's Lemma to show that $\dot{V}_4$ converges to zero and the error vector $(\mathbf{e}_1, \mathbf{e}_2, \theta_3, \mathbf{e}_4)$ converges to either $(\mathbf{0}, \mathbf{0}, 0, \mathbf{0})$ or $(\mathbf{0}, \mathbf{0}, \pi, \mathbf{0})$. For any initial conditions such that $V_4(0) < 2$, $\dot{V}_4$ is negative definite, implying that $(\mathbf{e}_1, \mathbf{e}_2, \theta_3, \mathbf{e}_4) = (\mathbf{0}, \mathbf{0}, 0, \mathbf{0})$ is uniformly asymptotically stable. □

The symmetry of the quadrotor dictates that rotations about the body z-axis are not constrained by the trajectory tracking objective and thus the third component of the torque $\boldsymbol{\tau}_z$ can be arbitrarily chosen to accomplish a secondary control objective. For the present case, we simply chose to drive the angular velocity $\boldsymbol{\omega}_z$ to zero, using for that purpose

$$\boldsymbol{\tau}_z = -k_z\boldsymbol{\omega}_z, \quad (72)$$

with $k_z > 0$.

3.3. Simulation results

The vehicles used in the simulations are all equal, with mass $m = 0.1$ kg and moments of inertia $I_{xx} = I_{yy} = 1 \times 10^{-3}$ kg m^2 and $I_{zz} = 2 \times 10^{-3}$ kg m^2. The products of inertia are assumed to be 0. These are typical values for very small scale vehicles, such as those used in the experimental test described in Section 4. To test the trajectory tracking controller, the gains and saturation parameters were set to $k_1 = 0.5$, $k_2 = 1.5$, $k_3 = 10$, $k_4 = 0.5$, $k_z = 1$, $K = 5$, and $c = 50$.

Trajectory tracking. In this simulation the quadrotor is set to track a planar trajectory described by (32) at a constant height $h = -1.5$ m. In order to demonstrate the performance of the controller, the quadrotor is initially placed at $\mathbf{p}(0) = [-5 \;\; 10 \;\; -10]^T$, with $\phi(0) = \pi$ and $\psi(0) = \theta(0) = 0$. The velocities (linear and angular) are initially zero. This is an extremely unfavorable configuration, in which the vehicle is turned upside down. As shown in Fig. 5 through the snapshots of the vehicle actuation taken at each second, the vehicle rapidly rotates to acquire an adequate attitude. The time evolution of the error $\mathbf{e}_3$ in Fig. 6 also shows a fast convergence of the error, which indicates an inversion in the direction of vector $\mathbf{r}_3$.

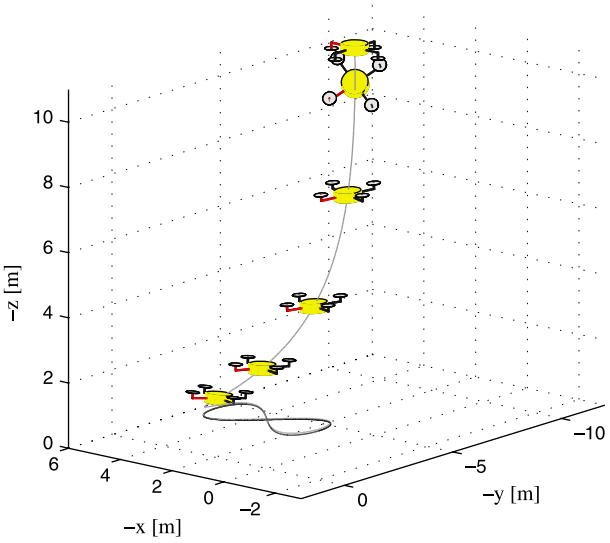

Fig. 5. Reference trajectory (black) and trajectory described by the vehicle (gray), with attitude snapshots every second for the first five seconds.

As shown in Fig. 6, all errors converge to zero as expected. During the first two seconds a faster convergence of the angular position and velocity errors $\mathbf{e}_3$ and $\mathbf{e}_4$ is observed, at the cost of some growth in the error $\mathbf{e}_2$. The position and velocity errors $\mathbf{e}_1$ and $\mathbf{e}_2$ have slower convergence rates and vanish to zero in approximately ten seconds.

Quadrotors in formation. In this simulation the leader, a quadrotor, is set to follow the same trajectory of the previous simulation. The motion of the leader (position, velocity, and acceleration) is provided to two follower quadrotors, which are supposed to follow the leader with identical d_x and symmetric d_y.

The quadrotors are initially at rest on the floor. The initial positions for the leader, follower 1, and follower 2 are $\mathbf{p}_L(0) = [0 \;\; 0 \;\; 0]^T$, $\mathbf{p}_{F1}(0) = [-0.5 \;\; -1 \;\; 0]^T$ and $\mathbf{p}_{F2}(0) = [-2 \;\; 1 \;\; 0]^T$, respectively. The selected distance vectors are $\mathbf{d}_1 = [0.35 \;\; 0.35 \;\; -0.3]^T$ and $\mathbf{d}_2 = [0.35 \;\; -0.35 \;\; -0.3]^T$. The control gains used for generating the reference trajectories are $k_1 = 0.2$, $k_2 = 2$, $k_3 = 0$, $k_{z1} = 0.2$, $k_{z2} = 2$, and $K = 5$.

To assess the robustness of the coordination strategy, noise was added to the state measurement of each quadrotor. As the trajectory generation depends on the leader's state, the addition of noise to the state indirectly introduces noise in the trajectory generation. The noise added is white Gaussian with zero mean and has a standard deviation of 0.2 m for the position, 0.1 m/s for the linear velocity, 0.01 m/s^2 for the acceleration, 0.02°/s for the angular velocity and 0.02° for the attitude measurement. These values are typical for low cost sensors.

The planar position plot in Fig. 7 shows the trajectory described by the leader, the reference trajectories described by the virtual vehicles, and the actual trajectories described by the follower vehicles. The triangles indicate the initial positions of the vehicles and the squares the positions at the end of the simulation. Fig. 7 shows that the trajectory generator is able to generate adequate reference trajectories at runtime and the quadrotors are able to track them, using the proposed trajectory tracking controller.

Fig. 8 shows the time evolution of the errors for the virtual vehicles. These are only plotted after $t \approx 10$ s, since the controllers

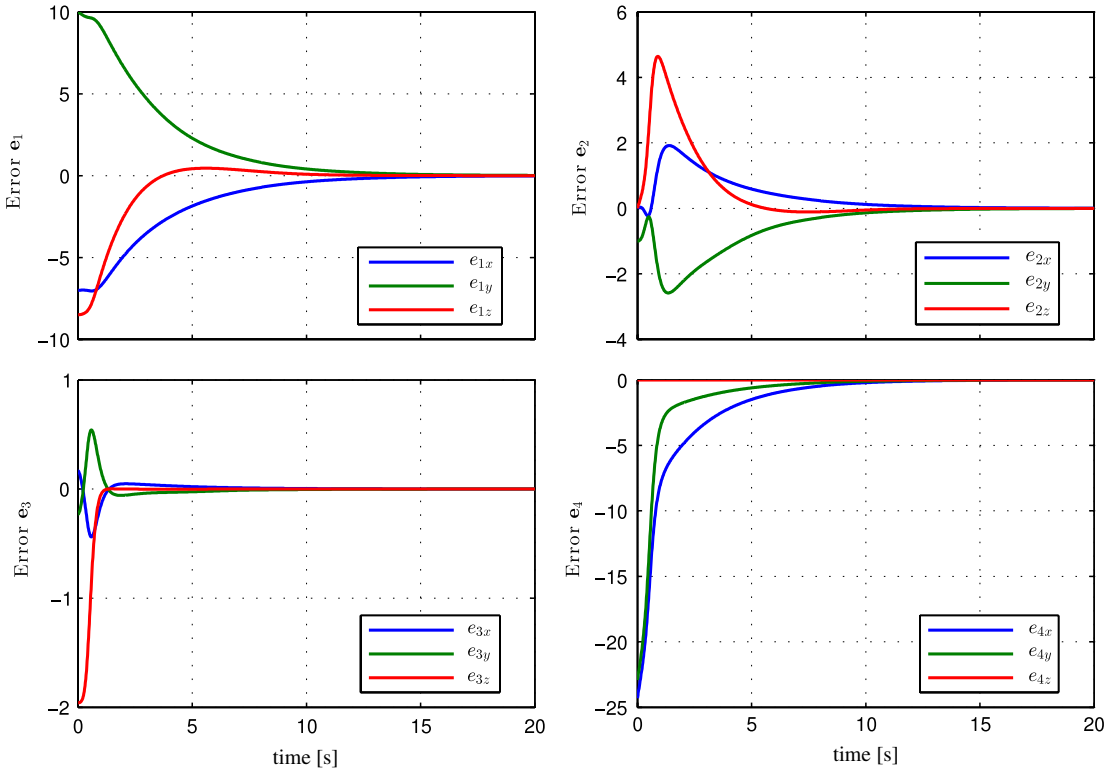

Fig. 6. Time evolution of the error coordinates.

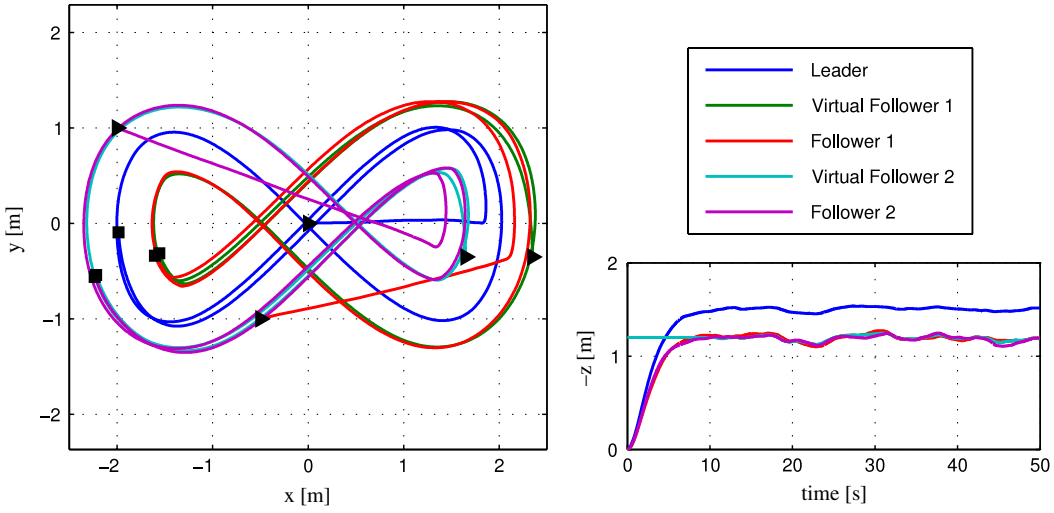

Fig. 7. Leader trajectory, generated trajectories, and follower trajectories.

are turned off before that moment. At the beginning, the vehicles rapidly converge to the starting points of the trajectories, while the trajectory generator is stopped. Once they approach these points the trajectory generator is started and the leader starts describing the figure eight trajectory.

The effect of noise on the trajectory generation is evidenced both in Fig. 8 and in the height plot shown in Fig. 7. Notice that the variations in height of the leader have repercussions in the time evolution of the followers' height. Nevertheless, the quadrotors were able to track the generated trajectories as shown in the plot of the errors in Fig. 9.

Lastly, Fig. 10 shows that the distance between quadrotors is kept approximately constant, not varying more than 0.1 m between leader and followers and 0.15 m between followers, which corresponds to approximately 20% of their average distance values.

4. Experimental evaluation

This section presents the results of an experimental test carried out at the Sensor-Based Cooperative Robotics Research Laboratory — SCORE Lab of the Faculty of Science and Technology of the University of Macau. A video with experimental results for the proposed leader–follower strategy is available at [24].

Three quadrotors Blade mQX [22] were used in the experiment. These vehicles weigh 78 g, have a length of 292 mm and are actuated in terms of thrust and angular velocity. They are designed to be human piloted with remote controls. However, it was possible to identify the radio chip inside the remote control and

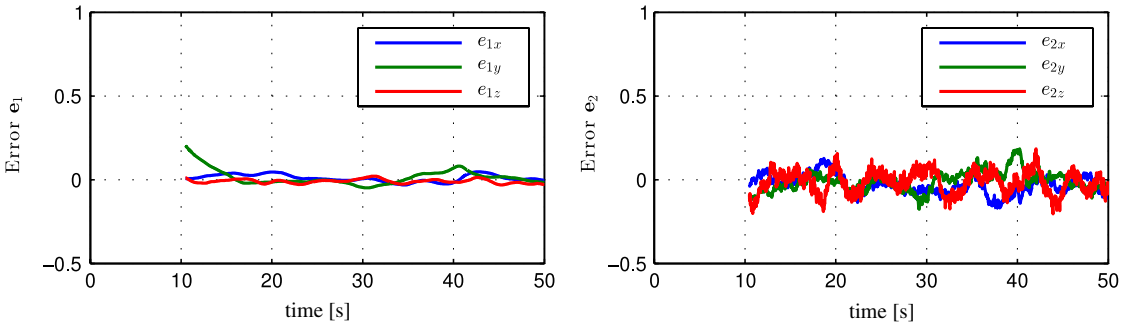

Fig. 8. Time evolution of the position errors for both virtual followers.

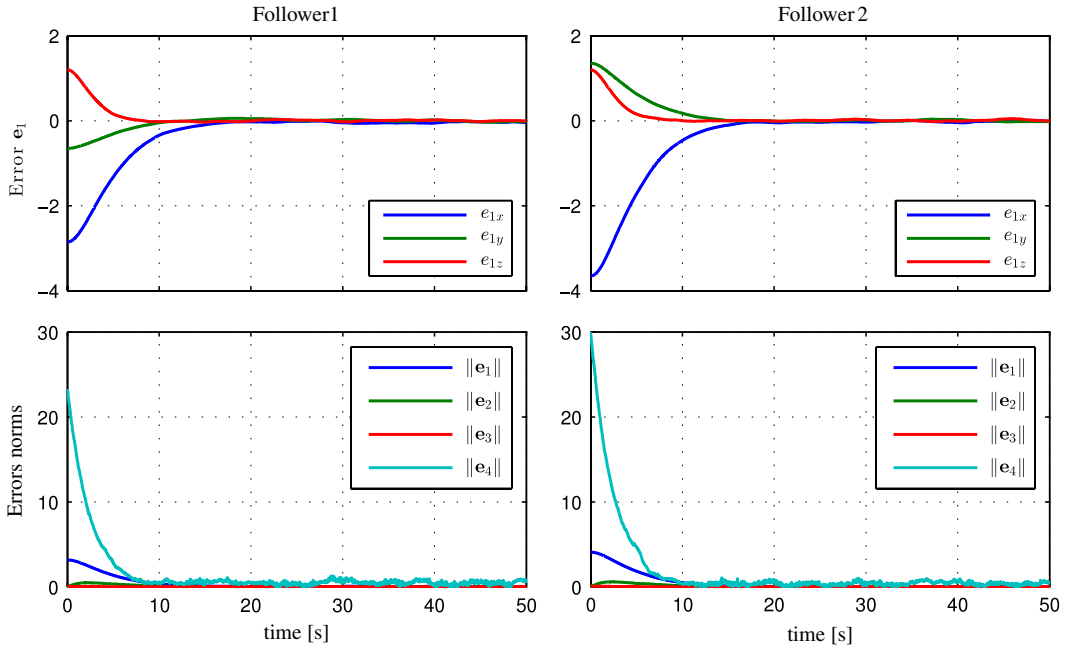

Fig. 9. Time evolution of the trajectory tracking errors for both followers.

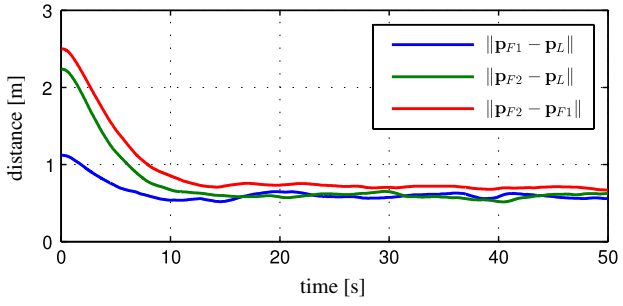

Fig. 10. Time evolution of the distance between leader and followers (and between them).

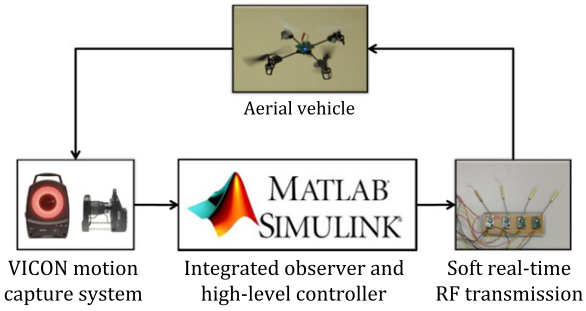

Fig. 11. System architecture.

connect the serial interface of the RF module to a computer serial port. A VICON motion capture system [21], composed of 12 high-speed high-resolution cameras and a set of markers attached to the plants, was used to capture the position and attitude of the vehicles at 50 Hz.

Two computers were used in this experiment, one running the VICON software and a Simulink control module, which generates the command signals, and a second one, which receives these commands through Ethernet and sends them through serial port to the RF module at 44 Hz. The decision to separate control and communications was made to avoid jitter in the transmission of the serial-port signals to the RF module. A block diagram of the overall architecture is presented in Fig. 11.

The control module implemented in Matlab/Simulink contains the trajectory generator for the two followers and the trajectory tracking controller for the three vehicles. This controller is an adaptation of the one presented in Section 3.2, with actuation in thrust and angular velocity rather than thrust and torque, given that the Blade mQX quadrotor is actuated in thrust and angular velocity. An inner-loop controller is responsible for tracking the angular velocity commands.

The VICON system outputs a pre-filtered position of the vehicle and with single differences it is possible to obtain a

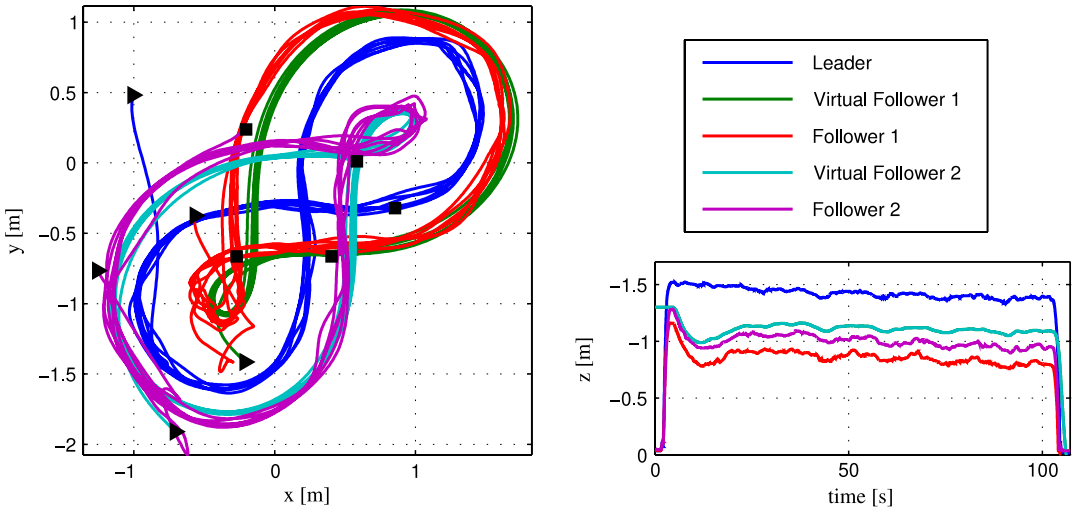

Fig. 12. Leader trajectory, generated trajectories, and follower trajectories.

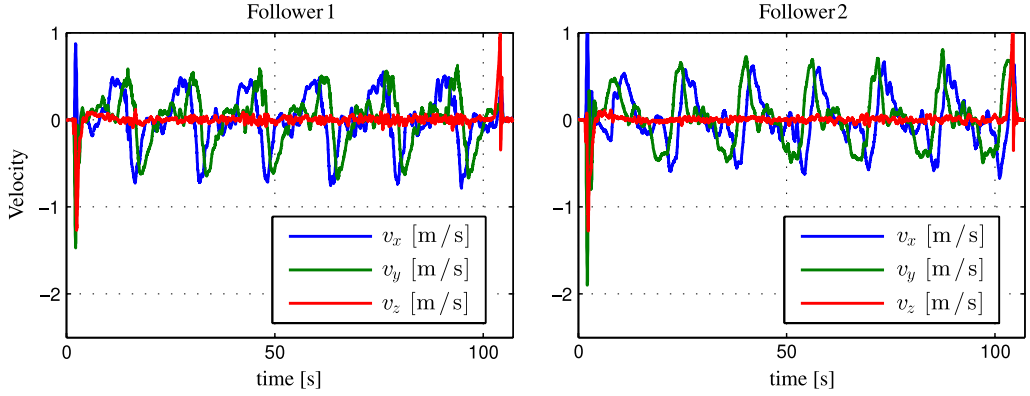

Fig. 13. Time evolution of velocities for both followers.

clean estimation of the velocity. However, double differences are highly contaminated with noise, degrading the quality of the estimated acceleration signals. To overcome this problem, we used a low-pass filter on the measurements. Using experimental data taken from earlier tests performed with a quadrotor, we tested the performance of various filters, with different dimensions. The best trade-off between responsiveness and smoothing was obtained with a moving average filter with 100 coefficients, which introduces a delay of approximately 1 s.

4.1. Results

In this experimental test, the leader is tracking a lemniscate trajectory given by

$$\mathbf{p}_L(\gamma) = \begin{bmatrix} \frac{3}{2}\frac{\sin(\gamma/3)}{1+\sin^2(\gamma/3)} \\ \frac{3}{4}\frac{\sin(2\gamma/3)}{1+\sin^2(\gamma/3)} \\ -1.6 \end{bmatrix} \tag{73}$$

where $\dot{\gamma} = \sqrt{1+\sin^2\gamma}$, which produces a trajectory with a constant linear speed. The trajectory is rotated by $\pi/4$ counter-clockwise, to take full advantage of the space available in the laboratory (see Fig. 12).

At the beginning of the test the quadrotors are at rest. The initial positions of the leader, follower 1, and follower 2 were $\mathbf{p}_L(0) = [-1 \;\; 0.48 \;\; 0]^T$, $\mathbf{p}_{F1}(0) = [-0.57 \;\; -0.37 \;\; 0]^T$, and $\mathbf{p}_{F2}(0) = [-1.26 \;\; -0.77 \;\; 0]^T$, respectively. The distance vectors $\mathbf{d}$ for each follower were $\mathbf{d}_1 = [0.35 \;\; 0.35 \;\; -0.3]^T$ and $\mathbf{d}_2 = [0.35 \;\; -0.35 \;\; -0.3]^T$. The control gains and saturation parameters used for the trajectory generator were $k_1 = 0.3$, $k_2 = 1.1$, $k_3 = 0.17$, $k_{z1} = 0.2$, $k_{z2} = 1$, and $p_{\max} = 5$.

Fig. 12 shows in separate plots the x–y plane view and the time evolution of the z-coordinate for the trajectory described by the leader, the reference trajectories described by the virtual vehicles, and the actual trajectories described by the follower vehicles. The triangles indicate the initial positions of the vehicles and the squares the positions at the end of the simulation. Fig. 12 shows that the trajectory generator is able to generate adequate reference trajectories and the quadrotors are able to track them, using the trajectory tracking controller proposed.

The generated reference trajectories capture the essence of leader's movement, while neglecting the higher frequency perturbations. For example in the z-coordinate plot, the longer and slower variations found in the leader's height can also be found in the height of the virtual followers. The high-frequency variations in the leader's height are filtered and do not appear in the generated trajectories. This process results in smoother trajectories that can be adequately tracked, as can be seen from the time evolution of velocities and trajectory tracking errors (see Figs. 13 and 14).

Fig. 15 shows the time evolution of the errors for the virtual vehicles, which exhibit an oscillatory behavior. This oscillation is a result of the trade-off that was found between mitigating the position error $\mathbf{e}_1$ and limiting the sensitiveness of the trajectories to the perturbations in leader's movement. It is possible to

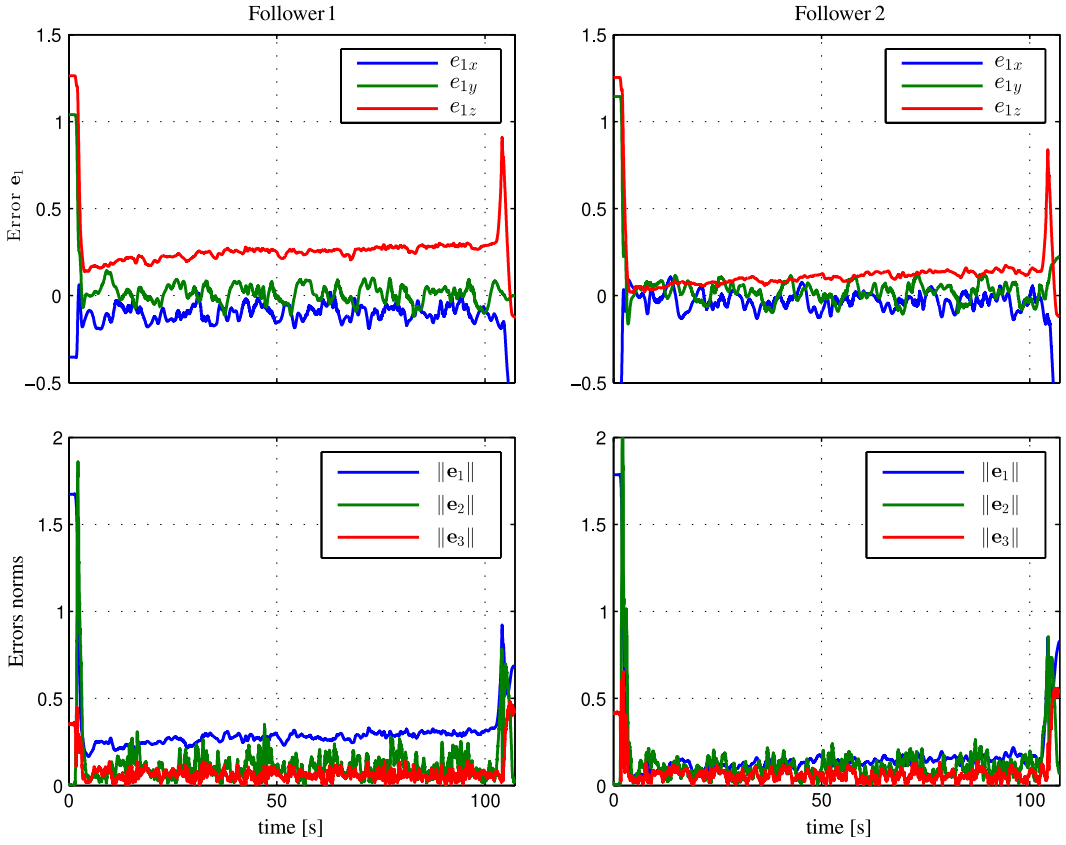

Fig. 14. Time evolution of the trajectory tracking errors for both followers.

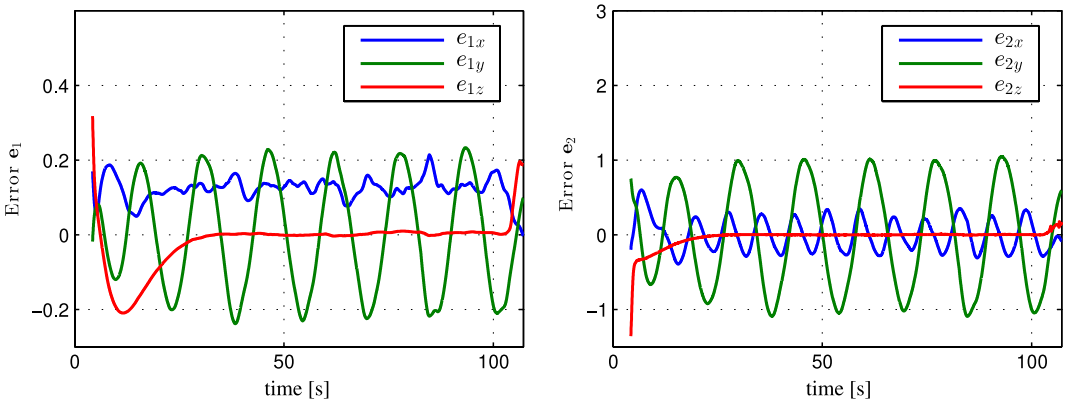

Fig. 15. Time evolution of the errors for both virtual followers.

maintain the virtual errors close to the origin, but at the cost of degrading the trajectory tracking performance.

5. Conclusion

This paper presented a strategy for the generation of formation trajectories for autonomous air vehicles. A leader–follower approach was adopted, which relies on a nonlinear control law to stabilize, at a predefined distance vector, the position of the leader in the body frame of a set of virtual followers. Global asymptotic stabilization of the leader–follower linear distance together with local boundedness of the leader–follower angular distances is guaranteed, provided that well-defined conditions relating the curvature of the leader's trajectory and the desired distances between vehicles are met. It has also been shown that when equal values for the desired longitudinal distance to the leader are used, the vehicles move in a rigid formation topology. For trajectory tracking control of quadrotor vehicles, a globally stabilizing controller that also guarantees the boundedness of the thrust actuation was proposed.

Both the simulation and experimental tests were performed to demonstrate the applicability of the method to the task of controlling quadrotors in formation, showing that the generated trajectories are easily tracked by the aerial vehicles. In spite of the fact that only the leader's position was being measured, the computation of smoothed single and double differences allowed for an adequate generation and accurate tracking of formation trajectories.

Directions for future work include investigating and deriving a formal proof for the conditions under which a group of followers converges to a rigid formation, extending the trajectory generator to natively generate three-dimensional trajectories

without decoupling the vertical component, and applying the proposed method to cascaded leader–follower formations.

Acknowledgment

This work was partly funded by Fundação para a Ciência e Tecnologia under the Projects PEst-OE/EEI/LA0009/2011 and SCARVE-PTDC/EEA-CRO/102857/2008.

References

[1] R.M. Murray, Recent research in cooperative control of multivehicle systems, Trans. ASME, J. Dyn. Syst. Meas. Control 129 (5) (2007) 571–583.
[2] P. Ogren, E. Fiorelli, N.E. Leonard, Cooperative control of mobile sensor networks: adaptive gradient climbing in a distributed environment, IEEE Trans. Automat. Control 49 (2004) 1292–1302.
[3] S. Waharte, N. Trigoni, S. Julier, Coordinated search with a swarm of uavs, in: 6th Annual IEEE Communications Society Conference on Sensor, Mesh and Ad Hoc Communications and Networks Workshops, 2009. SECON Workshops'09. 2009, pp. 1–3.
[4] N. Michael, J. Fink, V. Kumar, Cooperative manipulation and transportation with aerial robots, Auton. Robots 30 (1) (2011) 73–86.
[5] R. Olfati-Saber, Flocking for multi-agent dynamic systems: algorithms and theory, IEEE Trans. Automat. Control 51 (3) (2006) 401–420.
[6] E. Justh, P. Krishnaprasad, Equilibria and steering laws for planar formations, Systems Control Lett. 52 (1) (2004) 25–38.
[7] J. Guerrero, R. Lozano, Flight formation of multiple mini rotorcraft based on nested saturations, in: 2010 IEEE/RSJ International Conference on Intelligent Robots and Systems, IROS, 2010, pp. 634–639.
[8] T. Balch, R. Arkin, Behavior-based formation control for multirobot teams, IEEE Trans. Robot. Automat. 14 (6) (1998) 926–939.
[9] N. Leonard, E. Fiorelli, Virtual leaders, artificial potentials and coordinated control of groups, in: Proceedings of the 40th IEEE Conference on Decision and Control, vol. 3, 2001, pp. 2968–2973.
[10] R. Olfati-Saber, R.M. Murray, Distributed cooperative control of multiple vehicle formations using structural potential functions, in: 15th IFAC World Congress, vol. 15, 2002.
[11] J. Fax, R. Murray, Information flow and cooperative control of vehicle formations, IEEE Trans. Automat. Control 49 (9) (2004) 1465–1476.
[12] H. Tanner, G. Pappas, V. Kumar, Leader-to-formation stability, IEEE Trans. Robot. Automat. 20 (3) (2004) 443–455.
[13] L. Consolini, F. Morbidi, D. Prattichizzo, M. Tosques, On a class of hierarchical formations of unicycles and their internal dynamics, IEEE Trans. Automat. Control 57 (4) (2012) 845–859. http://dx.doi.org/10.1109/TAC.2011.2166299.
[14] Z. Peng, G. Wen, A. Rahmani, Y. Yu, Leader–follower formation control of nonholonomic mobile robots based on a bioinspired neurodynamic based approach, Robot. Autonom. Syst. 61 (9) (2013) 988–996.
[15] R. Cui, S.S. Ge, B.V.E. How, Y.S. Choo, Leader–follower formation control of underactuated autonomous underwater vehicles, Ocean Eng. 37 (17–18) (2010) 1491–1502.
[16] D.M. Stipanovic, G. Inalhan, R. Teo, C.J. Tomlin, Decentralized overlapping control of a formation of unmanned aerial vehicles, Automatica 40 (8) (2004) 1285–1296.
[17] M. Turpin, N. Michael, V. Kumar, Trajectory design and control for aggressive formation flight with quadrotors, Auton. Robots 33 (2012) 143–156.
[18] M. Krstic, I. Kanellakopoulos, P.V. Kokotovic, Nonlinear and Adaptive Control Design, Wiley, 1995.
[19] B. Vik, T. Fossen, A nonlinear observer for gps and ins integration, in: Proceedings of the 40th IEEE Conference on Decision and Control, vol. 3, 2001, pp. 2956–2961.
[20] D. Cabecinhas, R. Cunha, C. Silvestre, Saturated output feedback control of a quadrotor aircraft, in: American Control Conference, ACC, 2012, pp. 4667–4602.
[21] Vicon system, http://www.vicon.com/ (September 2012).
[22] Horizon hobby, http://www.horizonhobby.com/ (September 2012).
[23] V. Roldão, R. Cunha, D. Cabecinhas, P. Oliveira, C. Silvestre, A novel leader-following strategy applied to formation control of quadrotors, in: European Control Conference, ECC, 2013.
[24] Video of the leader-following experimental results, 2014. http://users.isr.ist.utl.pt/~rmac/SCARVE/videos/RAS2014.m4v.
[25] D. Cabecinhas, R. Cunha, C. Silvestre, Rotorcraft path following control for extended flight envelope coverage, in: Proceedings of the 48th IEEE Conference on Decision and Control, Held Jointly with the 28th Chinese Control Conference, 2009, pp. 3460–3465.
[26] F. Tyan, D.S. Bernstein, Global stabilization of systems containing a double integrator using a saturated linear controller, Internat. J. Robust Nonlinear Control 9 (15) (1999) 1143–1156.

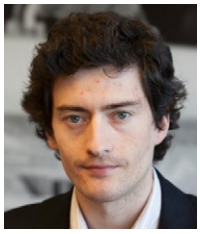

Valter Roldão received his M.Sc. degree in Aerospace Engineering from Instituto Superior Técnico (IST), Lisbon, Portugal, in 2012. He developed his research at the Institute for Systems and Robotics, Associated Laboratory for Robotics and Systems in Engineering and Science, Lisbon. His research interests include Robotics and Autonomous Vehicles with special focus on nonlinear control.

Rita Cunha received a Licenciatura degree in Information Systems and Computer Engineering and a Ph.D. degree in Electrical and Computer Engineering from the Instituto Superior Tecnico (IST), Technical University of Lisbon, Portugal, in 1998 and 2007, respectively. She is currently a Researcher with the Institute for Systems and Robotics, Associated Laboratory for Robotics and Systems in Engineering and Science, Lisbon, and she holds an Invited Assistant Professor position with the Department of Electrical and Computer Engineering of IST. Her research interests include guidance, navigation, and control of autonomous vehicles; nonlinear control; vision-based control; and modeling of small-scale helicopters and quadrotors.

David Cabecinhas received, in 2006, the Licenciatura degree in Electrical and Computer Engineering from Instituto Superior Técnico (IST), Lisbon, Portugal. From 2005 to 2006 he was Monitor in the Department of Electrical and Computer Engineering of IST and in 2007 he enrolled in the Ph.D. program at the same institution, developing his research at the Laboratory for Systems and Robotics in Engineering and Science, Lisbon. His current research interests include guidance, navigation, and control of autonomous vehicles, nonlinear control, vision-based control, and integration of vision and inertial sensors for attitude and position estimation.

Carlos Silvestre received the Licenciatura degree in Electrical Engineering from the Instituto Superior Tecnico (IST) of Lisbon, Portugal, in 1987 and the M.Sc. degree in Electrical Engineering and the Ph.D. degree in Control Science from the same school in 1991 and 2000, respectively. In 2011 he received the Habilitation in Electrical Engineering and Computers also from IST. Since 2000, he is with the Department of Electrical Engineering of the Instituto Superior Tecnico, where he is currently an Associate Professor of Control and Robotics in leave. Since 2012 he is an Associate Professor of the Department of Electrical and Computer Engineering of the Faculty of Science and Technology of the University of Macau. Over the past years, he has conducted research on the subjects of navigation guidance and control of air and underwater robots. His research interests include linear and nonlinear control theory, coordinated control of multiple vehicles, gain scheduled control, integrated design of guidance and control systems, inertial navigation systems, and mission control and real-time architectures for complex autonomous systems with applications to unmanned air and underwater vehicles.

Paulo Oliveira received the Ph.D. degree in 2002 from the Instituto Superior Técnico (IST), Lisbon, Portugal. He is currently an Associate Professor with the Department of Mechanical Engineering, Universidade de Lisboa, IST, Lisbon, Portugal and a Researcher with the Institute for Systems and Robotics, Associated Laboratory for Robotics and Systems in Engineering and Science, Lisbon, Portugal. His research interests include Robotics and Autonomous Vehicles with special focus on the fields of sensor fusion, navigation, positioning, and estimation. He has participated in more than 15 Portuguese and European Research projects over the last 20 years.